RSC Advances

PAPER

View Article Online
View Journal | View Issue

Cite this: *RSC Adv.*, 2021, **11**, 5008

The enhanced reduction of bromate by highly reactive and dispersive green nano-zerovalent iron (G-NZVI) synthesized with onion peel extract†

Olga Lem,[a] Sunho Yoon,[b] Sungjun Bae[b] and Woojin Lee[*a]

In this study, novel green nano-zerovalent iron (G-NZVI) is synthesized for the first time using onion peel extract for the prevention of rapid surface oxidation and the enhancement of particle dispersibility with a high reductive capacity. The results from various surface analyses revealed that the spherical shape of G-NZVI was fully covered by the onion peel extract composed of polyphenolic compounds with C=C–C=C unsaturated carbon, C=C, C–O, and O–H bonds, resulting in high mobility during column chromatography. Furthermore, the obtained G-NZVI showed the complete removal of 50 mg L^{-1} of bromate (BrO_3^-) in 2 min under both aerobic (k = 4.42 min^{-1}) and anaerobic conditions (k = 4.50 min^{-1}), showing that G-NZVI had outstanding oxidation resistance compared to that of bare NZVI. Moreover, the observed performance of G-NZVI showed that it was much more reactive than other well-known reductants (*e.g.*, Fe and Co metal organic frameworks), regardless of whether aerobic or anaerobic conditions were used. The effects of G-NZVI loading, the BrO_3^- concentration, and pH on the BrO_3^- removal kinetics using G-NZVI were also investigated in this study. The results provide the novel insight that organic onion peel waste can be reused to synthesize highly reactive anti-oxidative nanoparticles for the treatment of inorganic chemical species and heavy metals in water and wastewater.

Received 22nd November 2020
Accepted 12th January 2021

DOI: 10.1039/d0ra09897c

rsc.li/rsc-advances

Introduction

In the natural environment, a relatively high concentration of bromine (Br) has been frequently detected worldwide, for example in seawater (65–80 mg L^{-1}), in brines (200–300 mg L^{-1}), and in some salt lakes (2000–12 000 mg L^{-1}).[1–3] In addition, the increase in the concentration of bromide (Br^-) in drinking water is of interest because of the problems of salt-water intrusion.[4] Bromide has been also known as a main source of bromate (BrO_3^-) formation during water and wastewater treatment using an ozonation step, one of the main advanced oxidation processes (AOPs).[5] Because BrO_3^- is considered as a Group 2B carcinogen by the International Agency for Research on Cancer (IARC), the maximum acceptable level of BrO_3^- in drinking water has been set as 10 μg L^{-1} by the World Health Organization and European Commission.[5–7] Therefore, the detection of a high concentration of BrO_3^- is a great concern during water and wastewater treatment and its fate and transport in the water systems have attracted the interest of environmental scientists and engineers.

To eliminate BrO_3^- in water, three environmental strategic approaches have been generally introduced: (i) decrease of the Br^- input concentration before the formation of BrO_3^-, (ii) prevention of BrO_3^- formation during the AOP, and (iii) removal of BrO_3^- after the AOP. The first approach includes some unit environmental processes such as ion exchange, membrane filtration, and precipitation.[8] Although these unit processes can be properly managed by experienced environmental engineers under optimal operation conditions, it is very challenging to effectively and cost-efficiently remove Br^- where there are different environmental issues using the conventional processes.[9] The second one including the addition of NH_3 or H_2O_2, decrease of pH, use of hydroxyl radicals and HOBr scavengers, and hypobromous acid reduction has also experienced difficulties and serious drawbacks in effectively inhibiting the formation of BrO_3^- during the AOP.[10–14] The last approach focuses on the chemical reduction of BrO_3^- using photolysis, catalysis, and photocatalysis.[15] Compared to the simple reductive catalysis of BrO_3, its removal by the photolysis and/or photocatalysis, *e.g.*, UV light is uneconomical and its reaction kinetics are much slower.[16] In contrast, metal organic frameworks (MOFs) such as MIL-88A and ZIF-67 have recently been synthesized and applied to the catalytic reduction of BrO_3^-, resulting in complete removal in 1 h under aerobic conditions.[17,18] However, the synthesis of MOFs is quite an expensive

[a]*Department of Civil and Environmental Engineering, National Laboratory Astana, Nazarbayev University, Nur-Sultan 010000, Republic of Kazakhstan. E-mail: woojin.lee@nu.edu.kz; Tel: +7-7172-70-6540*

[b]*Department of Civil and Environmental Engineering, Konkuk University, Seoul 05029, Republic of Korea*

† Electronic supplementary information (ESI) available. See DOI: 10.1039/d0ra09897c

and complicated process for the mass production of an environmental catalyst for the treatment of BrO_3^- in the bulk water and wastewater systems. The Fe(III) coagulant and zerovalent iron (ZVI) have been also applied to BrO_3^- removal, which resulted in a limited removal efficiency and/or lower bromate reduction kinetics in conjunction with a rapid surface oxidation leading to significant damage to its durability and longevity for the continuous effective removal of aqueous bromate.[19,20]

In the last two decades, nano-ZVI (NZVI) has attracted great attention because of its outstanding reactivity for the removal of various redox vulnerable contaminants when compared to micro-ZVI. A well-known method for the NZVI synthesis uses sodium borohydride ($NaBH_4$) as a powerful reducing agent, for the reduction of Fe(II) and Fe(III) (eqn (1)):[21]

$$Fe(H_2O)_6^{3+} + 3BH_4^- + 3H_2O \rightarrow Fe^0\downarrow + 3B(OH)_3 + 10.5H_2 \quad (1)$$

However, the $NaBH_4$ showed a tendency to cause the aggregation of NZVI particles, leading to the decrease of its surface area and reactivity. To overcome the engineering hurdle, many organic surfactants such as sucrose, chitosan, and poly(vinylpyrrolidone) have been used as common coating chemicals of the NZVI surface to produce a high electrostatic repulsion on the surface and to avoid the aggregation of the NZVI particles.[22–25] Recently, researchers have developed a green synthesis method of NZVI, *i.e.*, green-NZVI (G-NZVI) using an environmentally friendly surface coating chemical obtained from plants, *e.g.*, polyphenols from green tea-sorghum or coffee.[26] In addition, some biochemical molecules from plant extracts such as proteins, polyphenols, and enzymes have even played a role as electron donor and/or mediator for the reduction of Fe(II)/Fe(III) to Fe(0) and these have been used as a coating material for the prevention of particle agglomeration too.[27,28]

Onion (*Allium cepa*) is a vegetable harvested worldwide and known as a healthy food source. However, its peel is usually thrown away as organic waste and it required that it be properly treated and managed in environmental treatment facilities, although the peel contains high concentrations of flavonoids and polyphenol compounds which can be a good source of surface coating chemicals for the synthesis of G-NZVI. In this study, natural polyphenols were extracted from the onion peel and used for the synthesis of highly anti-oxidative G-NZVI. Due to the relatively weak reduction potential of polyphenol, both natural polyphenol extract from the onion peel and a theoretically optimized amount of $NaBH_4$ (0.3 M) were tested to determine the proper synthesis method for reactive and dispersive G-NZVI. The newly synthesized G-NZVI was characterized by various surface analyses and its enhanced mobility in soil and groundwater systems were verified using a continuous column experiment. Batch kinetic tests were also conducted to characterize the reduction of aqueous BrO_3^- to Br^- by G-NZVI, and to investigate the effect of significant factors on the bromate removal kinetics at controlled experimental conditions, and to compare the reactivity of G-NZVI to those of conventional reducing agents (NZVIs and MOFs) reported previously. Finally, the potential reaction mechanism of the BrO_3^- reduction by G-NZVI is proposed in this paper.

Materials and experimental methods

Materials and chemicals

Potassium bromate (98%, ACS Grade Reagent, Sigma-Aldrich) and potassium bromide (99%, Sigma-Aldrich) were used to prepare the calibration standards for ion chromatography and stock solutions for the batch kinetic experiments. The $FeCl_3 \cdot 6H_2O$ (97%, Sigma-Aldrich), $NaBH_4$ (99%, Sigma-Aldrich), and extract of onion peel were used for the G-NZVI synthesis. Onion peel was obtained from a local market in Nur-Sultan city (Kazakhstan), and washed with deionized water (DIW) before polyphenol extraction. The H_2SO_4 (96%, ACS Grade Reagent, Sigma-Aldrich), $NaHCO_3$ (99%, ACS Grade Reagent, Sigma-Aldrich), and $NaCO_3$ (98%, ACS Grade Reagent, Sigma-Aldrich) were used as eluents for the ion chromatography (IC). The $FeCl_2$ (98%, Sigma-Aldrich) was used as a control for the homogeneous reduction of BrO_3^- by aqueous Fe(II). The HCl (37%, ACS Grade Reagent, Sigma-Aldrich) and NaOH (98%, Sigma-Aldrich) were used to adjust the pH for the evaluation of the pH effect on the BrO_3^- removal kinetics. Sand (50–70 mesh, Sigma-Aldrich) was used as a porous column medium for the column mobility test of G-NZVI. All the solutions were prepared with ultrapure DIW (18 MΩ cm, Millipore).

Synthesis of G-NZVI

To extract the polyphenols from onion peel, 12 g of onion peel was washed with DIW (400 mL) and boiled at 80 °C for 1 h. Then, the onion peel extract was vacuum filtered, and the filtrate was evaporated using a rotatory evaporator. The substance obtained was freeze dried using a vacuum freeze drier (Labconco, USA). The dried extract was weighed (4 g) and dissolved in 5 mL of DIW and stored at −4 °C until required. The G-NZVI was synthesized by adding 10 g L^{-1} of onion peel extract to 0.1 M of $FeCl_3$ solution (40 mL) at room temperature (20 ± 0.2 °C) under constant stirring for 15 min. An immediate color change from yellow to black was observed after adding the onion peel extract, indicating that the onion peel extract had reduced the Fe(III) to Fe(0). To accelerate and improve the reduction of Fe(III), 40 mL of $NaBH_4$ (0.3 M) was slowly added dropwise to the mixture of Fe(III) and onion peel extract under constant stirring for 15 min. After the formation of G-NZVI, all the synthesized G-NZVI particles were washed three times with deaerated deionized water (DDIW) to remove potential chemical impurities that remained on the G-NZVI surface. The slurry of G-NZVI was used for the batch kinetic experiments immediately after its synthesis or kept in an anaerobic chamber (Coy Laboratory Products, USA) for approximately two days to avoid an aging effect. Control materials (*i.e.*, G-NZVI synthesized without adding $NaBH_4$ (G-NZVI/NS) and bare NZVI without coating chemicals) were prepared to characterize the bromate reduction by G-NZVI by comparing its reactivity to those of the control materials. For the NZVI synthesis, the modified Wang's

synthesis method was followed, *i.e.*, mixing equal volumes of 0.1 M of $FeCl_3 \cdot 6H_2O$ and 0.3 M of $NaBH_4$.[29]

Characterization of G-NZVI

The morphology of G-NZVI was characterized by using scanning electron microscopy (SEM) coupled with energy dispersive X-ray spectroscopy (EDS) (Crossbeam 540, Zeiss, Germany). The crystalline characteristics of G-NZVI were identified using X-ray diffraction (XRD) (SmartLab, Rigaku, Germany) operating at 40 kV and 30 mA, with a scanning speed of 1° min^{-1} in a 2θ range of 10–80°. The X-ray photoelectron spectroscopy (XPS, K-Alpha, Thermo Fisher Scientific, USA) analysis was also conducted using a system equipped with a micro-focused monochromatic Al Kα X-ray source (1486.6 eV) (Sigma Probe, Thermo Fisher Scientific, USA). The IR spectra of G-NZVI and polyphenol from the onion peel extract were obtained using Fourier-transform infrared spectroscopy (FTIR, Thermo Fisher Scientific, USA). The pore size and surface area of the nanoparticles were measured by Brunauer–Emmett–Teller (BET) theory using a surface area and porosity analyzer (TriStar II, Micromeritics, USA). The mass percentage of an organic layer of G-NZVI was measured using a thermogravimetry and differential scanning calorimetry (TG-DSC) analyzer (STA 6000, PerkinElmer, USA).

Experimental procedures

All the batch kinetic experiments for the BrO_3^- removal by G-NZVI were conducted in 20 mL amber vials equipped with open-top caps and Teflon-faced rubber septa. The reaction was initiated by spiking the G-NZVI suspension with the stock BrO_3^- solution to prepare an initial concentration of BrO_3^- of 50 mg L^{-1} and 200 mg L^{-1} of G-NZVI. The reactants were mixed on a shaker at 50 rpm. Batch kinetic experiments were conducted under aerobic and anaerobic conditions. For the aerobic experiment, all the reactions were performed using DIW without considering air intrusion into the experiment, whereas DDIW was used for the preparation of anaerobic samples and their reactions were performed in an anaerobic chamber to avoid air intrusion. Control experiments were conducted to characterize the diverse removal kinetics of BrO_3^- by each type of reductant under aerobic conditions (G-NZVI/NS, G-NZVI, Fe(II), NZVI, and polyphenols). All the experiments were conducted in triplicate, unless otherwise specified.

To examine the effect of significant operation factors such as G-NZVI loading, BrO_3^- concentration, and suspension pH on the removal kinetics of the bromate, a batch kinetic test was run to determine the bromate removal, by varying one factor at a time under controlled experimental conditions. Firstly, the batch kinetic test was conducted to check the effect of G-NZVI loading on the bromate removal kinetics by varying its loadings in the range of 50–300 mg L^{-1} under controlled experimental conditions. The effect of BrO_3^- concentration on the kinetics was subsequently investigated by varying its concentration in the range of 50–200 mg L^{-1} under the experimental conditions with an optimal G-NZVI loading. Finally, the effect of the suspension pH on the BrO_3^- reduction was examined by varying the pH from 3 to 11 under conditions which were optimal for G-NZVI loading and BrO_3^- concentration. The suspension pH was adjusted using 0.1 M HCl and 0.1 M NaOH solutions. To monitor the removal of BrO_3^- and formation of Br^- in the G-NZVI suspension and to measure their concentrations at each sampling time, an IC (930 Compact IC Flex, Metrohm, Switzerland) was used with a Metrosep A Supp 4-250/4 column and conductivity detection was used. To check the mobility of G-NZVI and bare NZVI, a continuous column test was conducted using a column (3 cm inner diameter × 20 cm height) packed with sand. Two column reactors were fed with 500 mL of G-NZVI and bare NZVI suspensions (1 g L^{-1}) at a feeding rate of 0.1 mL s^{-1} (Fig. S1, ESI†), and effluent from both the columns was collected in glass bottles.

Results and discussion

Characterization of G-NZVI

The morphology of NZVI, G-NZVI, and G-NZVI/NS were characterized by SEM/EDS analysis (Fig. 1). The SEM image of bare NZVI (Fig. 1(a) and S2(a), ESI†) shows the spherical shape of the nanoparticles (<100 nm) with typical chain-like aggregates because of the high surface energy and the magnetic interaction of the NZVI particles.[30] In contrast, the SEM image of G-NZVI (Fig. 1(b) and S2(c),† SEM) shows the spherical shape of the nanoparticles (<100–600 nm) mixed with organic components from the onion peel extract. The G-NZVI/NS aggregates had an irregular rectangular shape (Fig. 1(c)), suggesting that the absence of $NaBH_4$ led to the potential formation of MOF between iron and polyphenols. However, the addition of $NaBH_4$ to the iron and polyphenols from the onion peel extract could cause a keto–enol transformation and subsequently reduce Fe(III) to Fe(0) during the synthesis of G-NZVI, resulting in the formation of different structures.[31] The EDS analysis (Fig. S2(d), ESI†) further confirmed the presence of Fe, showing an elemental composition of oxygen (18.4 ± 0.2%), carbon (25.5 ± 0.2%), and iron (55.5 ± 0.2%). The high content of carbon on the surface of G-NZVI originated from the polyphenols of the onion peel extract, and was much higher than that of the bare NZVI surface (1.8 ± 0.1%) (Fig. S2(b), ESI†).

Fig. 1(d) shows the XRD diffractograms of NZVI, G-NZVI, and G-NZVI/NS. In the NZVI sample, the peaks of lepidocrocite (FeOOH, $2\theta = 38.1^\circ$), Fe(0) ($2\theta = 44.5^\circ$ and 65.05°), and Fe(II)O ($2\theta = 77.8^\circ$) were observed, which were typically observed on the surface of bare NZVI.[32] In contrast, the diffractogram of G-NZVI/NS revealed peaks of Fe_2O_3 ($2\theta = 32^\circ$), FeOOH ($2\theta = 41^\circ$), and ferrocene ($C_{10}H_{10}Fe$, $2\theta = 45.5^\circ$), indicating that the onion peel extract alone could not fully reduce Fe(III) to Fe(0) during the synthesis.[33] However, no crystalline characteristics of the G-NZVI sample were observed because of its amorphous structure and any formation of iron oxy-hydroxides was due to the high reductive capacity combined with the polyphenols and $NaBH_4$ during the G-NZVI synthesis. To investigate oxidation states of Fe and C on the surface of G-NZVI, XPS analysis was used (Fig. 2). The Fe 2p profiles of bare NZVI (Fig. 2(a)) showed peaks at 706.5, 709.97, and 712.48 eV, corresponding to the binding energies of Fe(0) (706.5–707 eV), FeO (709–709.5 eV), and Fe_2O_3 (711–714 eV), respectively, whereas only the peaks at

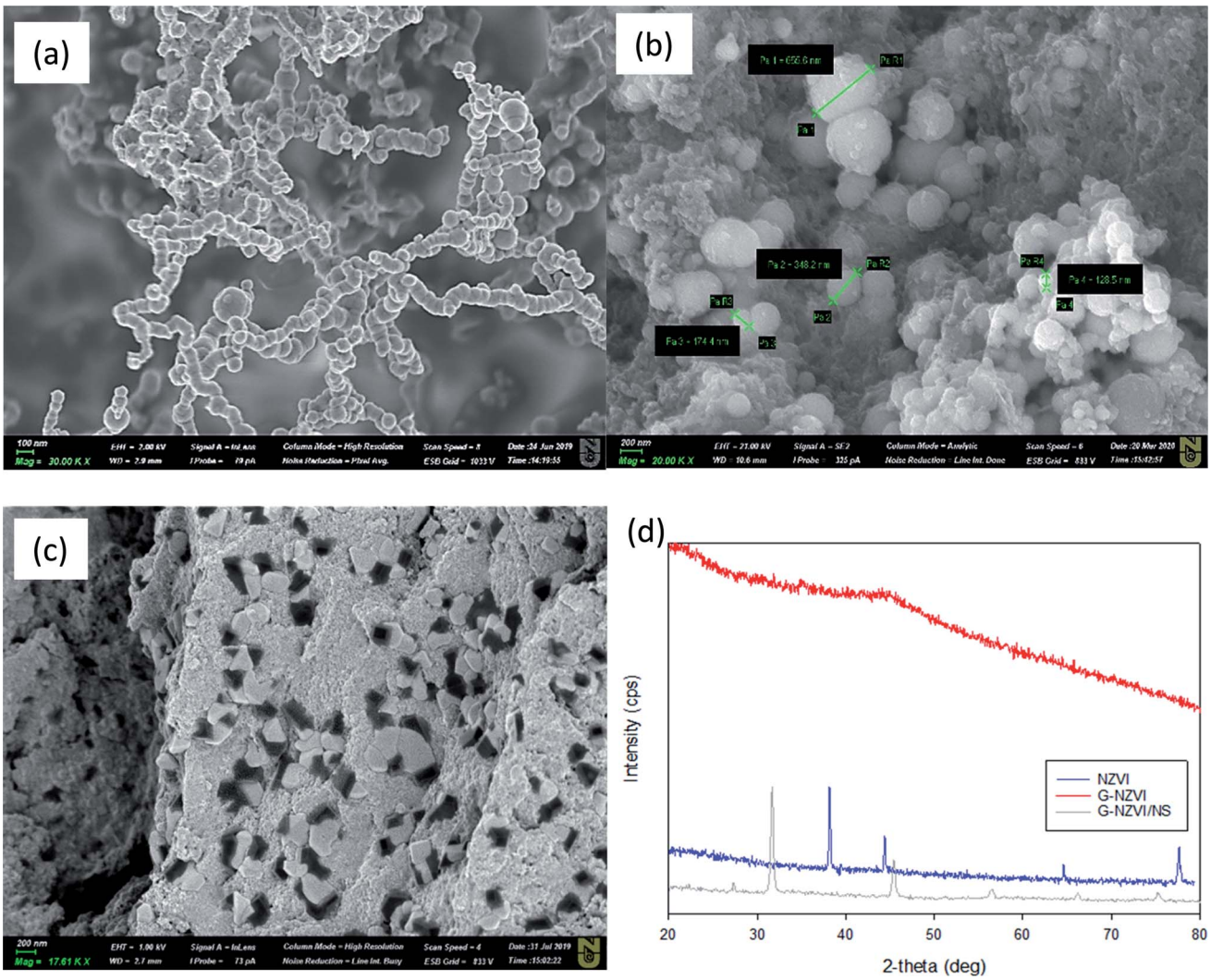

Fig. 1 SEM images of bare NZVI (a), G-NZVI (b), and G-NZVI/NS (c), and their XRD diffractograms (d).

711.32 and 713.46 eV for the G-NZVI were observed (Fig. 2(b)), indicating no Fe(0) was detected and this was probably due to the high content of the polyphenol coating on the surface of G-NZVI.[34,35] The C1s profile of G-NZVI (Fig. 2(e)) exhibited four different peaks at 284.97, 286.66, 288.61, and 290.20 eV, whereas only one clear C peak at 285 eV was observed in bare NZVI which came from the carbon tape used for the XPS analysis (Fig. 2(d)). The new peaks higher than 285 eV in the G-NZVI could be associated with unfunctionalized aromatic carbons, which belong to the phenolic rings.[36] A major C1s peak showed a positive binding energy shift of 1.6 eV, corresponding to the C–O–C and C–O–H functional groups.[36] The minor C1s peaks showing a positive binding energy shift of 3.61–4.2 eV corresponded to the O–C–C*=O and HO–C=O functional groups.[36] Therefore, all of the XPS results clearly showed that G-NZVI was fully associated with the various carbon functional groups of polyphenols from the onion peel extract.

Fig. 3 shows the FTIR spectra of NZVI, onion peel extract, and G-NZVI in the range of 400 to 4000 cm^{-1}. The FTIR spectrum of the onion peel extract showed bands at 3219.82 cm^{-1} (O–H stretching vibrations), 2329.45 cm^{-1} (C=C–C=C unsaturated carbon stretching), 1595.96 cm^{-1} (C=C stretching vibrations), 1499.1 cm^{-1} (O–H bending vibrations), 1367.34 cm^{-1} (C–O stretching of the ester group), 1249.36 cm^{-1} (C–O asymmetric stretching in cyclic polyphenolic compounds), and 1066.14 cm^{-1} (O–H deformation).[31] Similarly, the FTIR spectrum of G-NZVI revealed the presence of O–H stretching vibrations, C=C–C=C unsaturated carbon stretching, C=C stretching vibrations, C–O asymmetric stretching, and O–H deformation, which indicated that the surface of G-NZVI was fully coated by the onion peel extract composed of polyphenol substances. In contrast, the FTIR spectrum of NZVI did not show any presence of organic compound peaks. To quantify the amount of carbon coating on the surface of G-NZVI, TGA analysis was further performed the (Fig. S3, ESI†). Before the analysis, samples were freeze-dried to remove water molecules and no significant mass loss of samples occurred at temperatures lower than 100 °C. The profile of NZVI shows a steady increase in the mass, indicating the oxidation of zerovalent iron to iron oxides.[32] The thermal profile of onion peel extract showed that

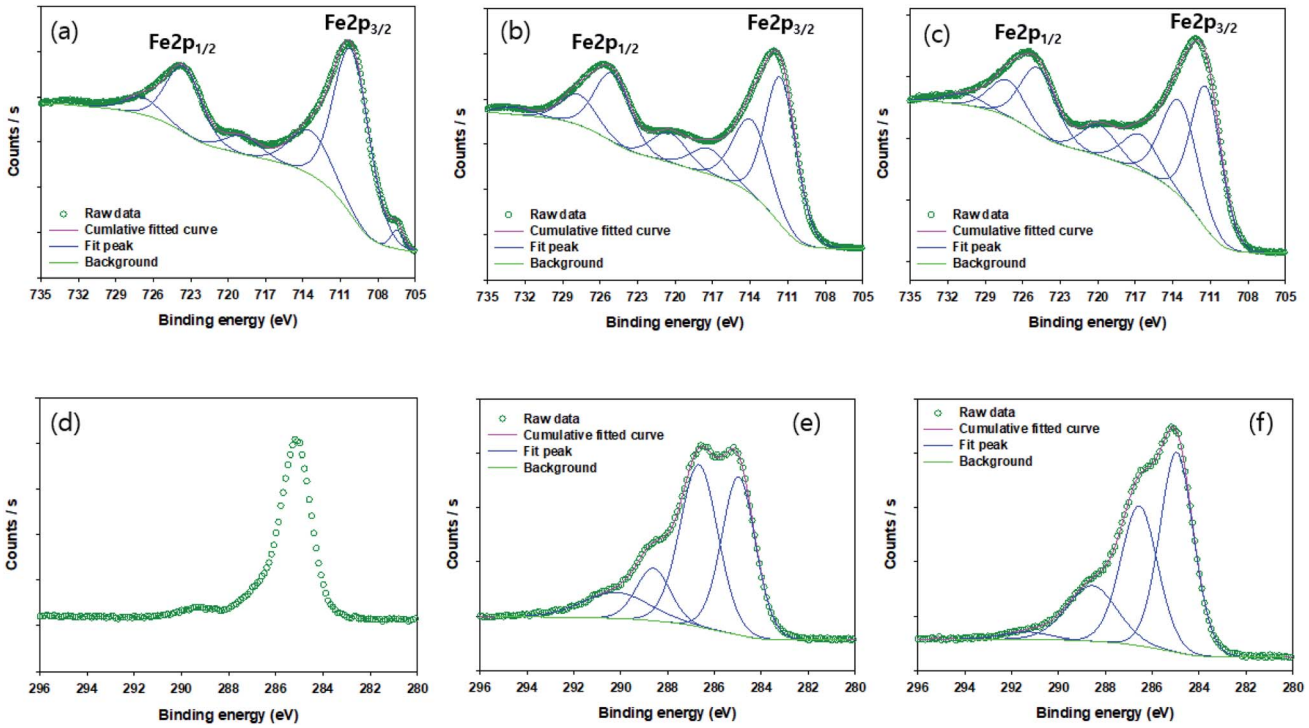

Fig. 2 The XPS spectra of iron and carbon on the surface of NZVI before BrO_3^- reduction (a and d), those of G-NZVI before the reaction (b and e), and those of G-NZVI after the reaction (c and f).

its mass loss due to the combustion of polyphenols started to occur as the temperature increased, at 130 °C. The G-NZVI sample retained approximately 60% of its initial mass at temperatures range than 130 °C, indicating that the organic coating layer of G-NZVI was almost 40% of the total mass of the nanoparticles.

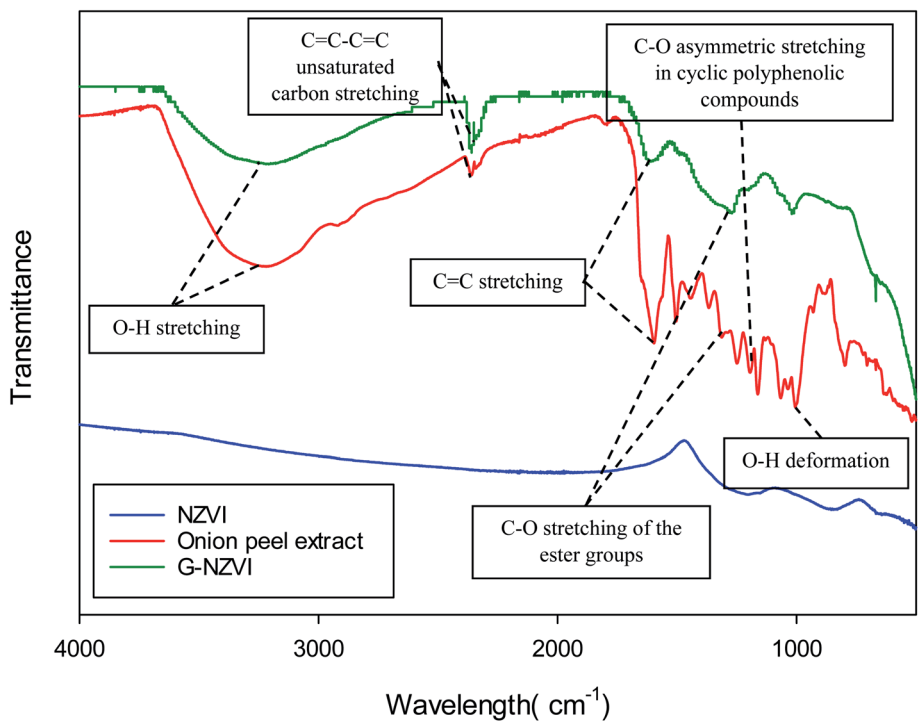

Fig. 3 The FTIR spectra of the onion peel extract, NZVI, and G-NZVI.

To evaluate the dispersibility and mobility of G-NZVI in soil and groundwater systems, a sand column test was conducted by injecting 500 mL of G-NZVI and NZVI suspensions into the columns for 1 h. The column with the bare NZVI suspension showed inferior dispersibility and mobility of NZVI during the continuous column test. The NZVI particles could not easily penetrate the porous sand column and were stuck at a depth of 2 cm from the top (Fig. 4(a)), whereas the G-NZVI particles completely passed through the column during the addition of the G-NZVI suspension (Fig. 4(b)). The presence of G-NZVI particles in the effluent and the increase of its loading in the glass bottle for the effluent collection as the column test was proceeded, could be clearly observed. The behavior of G-NZVI in the mobility and dispersibility of nanoparticles was remarkable compared to the behavior of bare NZVI in the porous sand column showing the absence of NZVI particles in its effluent (Fig. 4(c)). The enhanced mobility of G-NZVI exhibited in the porous sand column test could be caused by a steric repulsion due mainly to the coordination of polyphenol compounds from the onion peel extract on the surface of G-NZVI.[31]

Reduction of BrO_3^- by G-NZVI under aerobic and anaerobic conditions

Under aerobic conditions, almost no removal of BrO_3^- was observed in the control experiment with DIW (Fig. 5), showing that losses of BrO_3^- caused by volatilization and/or sorption on the glass wall of reactor were negligible in this study. No significant removal of BrO_3^- (2–5%) was observed in the aqueous solutions of onion peel extract and Fe(II) in 30 min. The Gibbs free energy values of diverse chemical species given in Table S1 (ESI†) showed that polyphenols could reduce Fe(III)/Fe(II) to Fe(0), whereas both polyphenols and Fe(II) could hardly reduce BrO_3^-, which was similar to previous observations. In contrast, the reduction of BrO_3^- occurred in the suspensions of G-NZVI, NZVI, and G-NZVI/NS, which was supported by the negative values of the Gibbs free energy change for the reactions between Fe(0) and BrO_3^- (Table S1, ESI†). Approximately, 40% of BrO_3^- was removed by G-NZVI/NS in 30 min, whereas a complete removal was observed in G-NZVI and NZVI suspensions in 2 min and 15 min, respectively. The removal kinetics were fitted by the pseudo-first-order and second-order rate laws and their kinetic models are:

$$\ln\left(\frac{C_0}{C}\right) = k_1 t \quad (2)$$

$$\frac{1}{C} = \frac{1}{C_0} + k_2 t \quad (3)$$

where C_0 is the initial concentration of BrO_3^-, C is the concentration of BrO_3^- at a specific time, k_1 is the pseudo-first-order rate constant (min^{-1}), k_2 is the second-order rate constant ($M\ min^{-1}$). Generally, the pseudo-first-order model showed a better fitting result in this study (Table S2†). In addition, the highest k_1 value ($4.42\ min^{-1}$) was obtained for the bromate removal from the G-NZVI suspension, which was almost 105 and 46 times higher than those from the suspensions of G-NZVI/NS ($0.042\ min^{-1}$) and NZVI ($0.095\ min^{-1}$), respectively. The enhanced performance by G-NZVI could be mainly caused by a high resistivity of G-NZVI against its surface oxidation despite the aerobic conditions throughout the batch kinetic test, when compared to that for bare NZVI. Furthermore, the specific surface area of G-NZVI ($59.7\ m^2\ g^{-1}$) was almost four times higher than that of bare NZVI ($13.8\ m^2\ g^{-1}$), which could possibly lead to the higher reductive capacity of G-NZVI for bromate removal.[37] The addition of polyphenols from onion peel extract during the synthesis of G-NZVI may facilitate the nucleation of iron nanoparticles by avoiding their agglomeration due to magnetism and thereby increase the surface area of G-NZVI during its crystal growth.[38]

Fig. 6 shows the comparison of the BrO_3^- removal kinetics in the suspensions of NZVI and G-NZVI under aerobic and anaerobic conditions. As shown for bare NZVI, a ~12 times

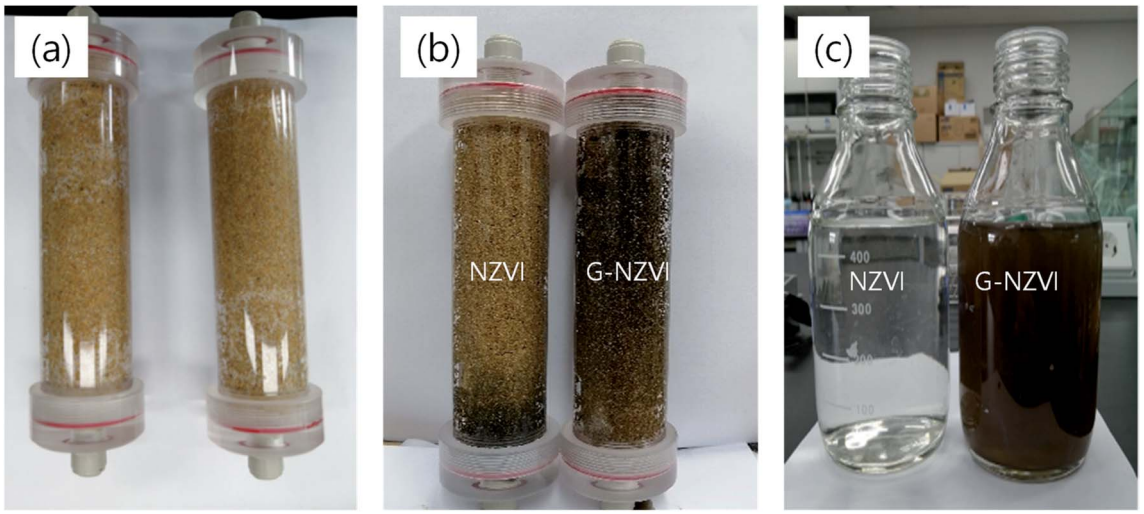

Fig. 4 Continuous column reactor testing to check the mobility and dispersibility of NZVI and G-NZVI: columns before the addition of the suspensions (a) and 1 h after the addition (b), and the collected effluents after passing through the columns (c).

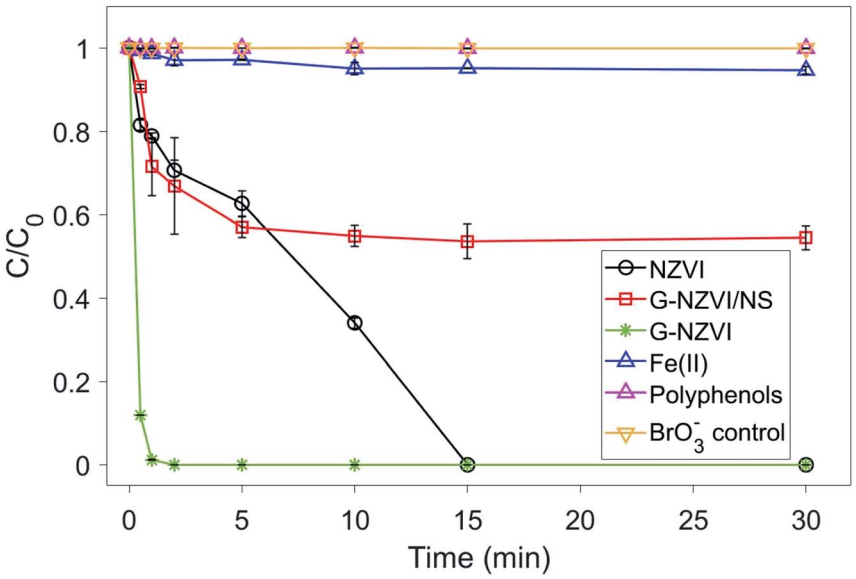

Fig. 5 The BrO_3^- reduction kinetics using five types of controls under aerobic conditions. Material loading: 200 mg L^{-1} and BrO_3^- concentration: 50 mg L^{-1}.

lower k_1 value (0.095 min^{-1}) was obtained in an aerobic NZVI suspension than that in an anaerobic NZVI suspension (1.196 min^{-1}) due to the rapid oxidation of the NZVI surface by competing oxy-anions in the aerobic NZVI suspension. Interestingly, the k_1 value of G-NZVI obtained under both aerobic (4.42 min^{-1}) and anaerobic (4.5 min^{-1}) conditions were very similar, indicating the high resistivity of G-NZVI against its surface oxidation by the coating of polyphenols. In addition, Table 1 shows that the enhanced reduction kinetics of BrO_3^- by G-NZVI were much faster than those of other reductants and catalysts such as NZVI supported on mesoporous silica, ethanol modified NZVI, and MOFs coordinated with Co and Fe metals. The k_1 value of G-NZVI was 16.9 times greater than that of mesoporous silica supported NZVI and 26.1 and 9.2 times greater than those of ZIF-67 (Co) and ZIF-67 (Fe), respectively, showing its superior reactivity for the reduction of BrO_3^-. In addition, the amount of G-NZVI (1 : 4) required to remove bromate was much smaller than that of NZVI (1 : 100). Because several tonnes of NZVI were applied at the practical treatment sites in the USA and Europe,[39] the reactive and eco-friendly G-NZVI may show higher cost effectiveness for the removal of aqueous BrO_3^- in water and wastewater treatment processes.

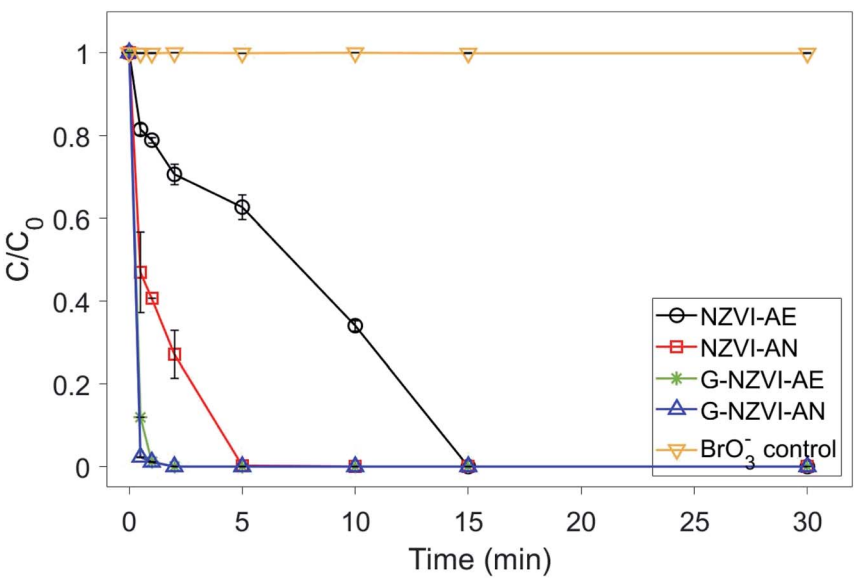

Fig. 6 The BrO_3^- reduction kinetics of using G-NZVI and NZVI under aerobic and anaerobic conditions. Material loading: 200 mg L^{-1}, BrO_3^- concentration: 50 mg L^{-1}.

Table 1 A comparison of the reactivity of G-NZVI with different catalysts and reducing agents

Type of catalyst	Bromate loading (mg L^{-1})	Catalyst loading (mg L^{-1})	Bromate to catalyst ratio	Reaction rate constant (min^{-1})	Reduction efficiency (time)	Conditions
NZVI on meso-porous silica[44]	0.2	25	1 : 125	0.0712	80% (4 h)	Anaerobic, 25 °C
Ethanol-modified NZVI[45]	1	100	1 : 100	0.0025[a]	99% (20 min)	Anaerobic, 25 °C
ZIF-67 (Co) + $NaBH_4$ (ref. 18)	100	250	1 : 2.5	0.046	100% (1 h)	Aerobic, 25 °C
MIL-88A (Fe) + $NaBH_4$ (ref. 17)	100	500	1 : 5	0.53	100% (1 h)	Aerobic, 25 °C
ZIF-67 (Fe) + $NaBH_4$ (ref. 17)	100	500	1 : 5	0.13	50% (1 h)	Aerobic, 25 °C
G-NZVI (this study)	50	200	1 : 4	1.2	100% (2 min)	Aerobic, 25 °C

[a] Second-order rate constant (M min^{-1}).

Fig. 7(a) shows the morphological change of G-NZVI after the BrO_3^- reduction. Spherically shaped nanoparticles can still be observed and newly formed plate-like nanoparticles can be seen after the BrO_3^- reduction by G-NZVI. One of XPS scan results (Fe2p spectra) of G-NZVI after the reaction showed peaks at 711.22 and 713.11 eV with a ratio of 1 : 0.67 (Fig. 3(c)), which was slightly comparable with the ratio before the reaction (1 : 0.56) indicating that the surface Fe was oxidized to Fe(III) after the BrO_3^- reduction.[35] For the C1s spectra of G-NZVI before the reaction, four different peaks were observed at 284.97, 286.66, 288.61, and 290.20 eV with a ratio of 0.87 : 1 : 0.29 : 0.28, whereas the peaks at 284.96, 286.56, 288.57, and 291.38 eV with a ratio of 1 : 0.76 : 0.41 : 0.05 were detected after the reaction. This indicated that the proportion of C–O–C, C–O–H, O–C–C*=O, and HO–C=O functional groups on the surface of G-NZVI decreased after the BrO_3^- reduction. The decrease of the proportion could be caused by changes in the structure of the polyphenols during the bromate removal, *i.e.*, keto–enol transformation by the redox reaction between polyphenols on the surface of G-NZVI and BrO_3^-. During the bromate reduction *via* electron transfer from G-NZVI, the polyphenols on its surface could be also reduced and transformed to the ketone and/or aldehyde containing molecules shown as plate-like nanoparticles in Fig. 7(a).[32] In addition, the FTIR spectrum of G-NZVI after the reaction showed a decrease in the intensity of the peak at 1271.85 cm^{-1} for C–O asymmetric stretching in cyclic polyphenolic compounds (Fig. 7(b)), which also supports the occurrence of keto–enol transformation in the polyphenols on the surface of G-NZVI during the reaction.[32] Based on the results obtained previously, the enhanced BrO_3^- removal by the G-NZVI particles could be explained by a two-step reaction. Firstly, due to the electrostatic attraction, BrO_3^- can be adsorbed on the reactive sites of G-NZVI in its suspension. Secondly, BrO_3^- can be reduced to Br^- *via* the electron transfer from the G-NZVI surface. It was observed that ~100% of the BrO_3^- reduction to Br^- by G-NZVI occurred during the reaction (Fig. S4(c)†). The corrosion rate of the surface Fe(0) of G-NZVI could be determined by the electron loss or gain process. The high oxidation resistivity of G-NZVI could be obtained from the polyphenol coatings of the onion peel extract on the G-NZVI surface, which could be another potential source of electrons during the keto–enol transformation.

Effects of significant experimental factors on the bromate removal kinetics

Fig. S4(a) (ESI)† shows the removal kinetics of BrO_3^- (50 mg L^{-1}) by G-NZVI at four different loadings of G-NZVI (50,

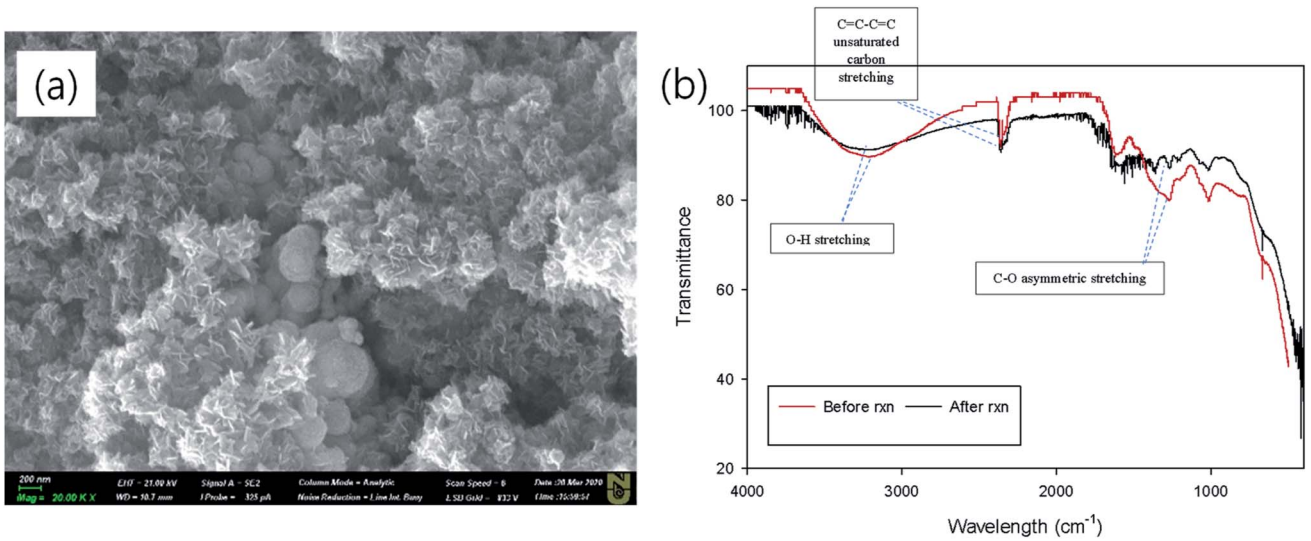

Fig. 7 SEM image (a) and FTIR spectra (b) of G-NZVI after BrO_3^- reduction.

100, 200, and 300 mg L^{-1}). As the G-NZVI loading increased from 50 to 300 mg L^{-1}, the removal efficiency of BrO_3^- and the k_1 values gradually increased from 10% to 100% and from 0.006 min^{-1} to 4.5 min^{-1}, respectively (Fig. S4(b) and Table S2, ESI†). The reductive transformation of organic and inorganic chemicals did not occur significantly in homogeneous aqueous reducing solutions but mostly occurred on the heterogeneous reactive surface of the solid reductants.[40] As the loading of G-NZVI increased in the suspension, it could provide more reactive sites on the surface of G-NZVI for the enhanced reduction of BrO_3, leading to the acceleration of the bromate reduction kinetics.[21]

Fig. S5(a) (ESI)† shows the removal kinetics of BrO_3^- by G-NZVI (200 mg L^{-1}) at four different concentrations of BrO_3^- (50, 75, 100, and 200 mg L^{-1}). At 50 mg L^{-1} of BrO_3^-, the complete removal of BrO_3^- was observed in 2 min, whereas the bromate removal efficiency gradually decreased as the concentration of the BrO_3^- increased. The k_1 values at a concentration of 50 mg L^{-1} of BrO_3^- was the highest and showed a dramatic decrease by ~12.5 times at 75 mg L^{-1} and the slow and gradual decrease was retained as the BrO_3^- concentration increased (Fig. S5(b) and Table S2, ESI†). This could be attributed to a limited reductive capacity of G-NZVI at a controlled constant loading and much faster oxidation of the G-NZVI surface at a higher concentration of BrO_3^-. The BrO_3^- removed during the reactions with G-NZVI was almost completely reduced to Br^- in all of the experiments (Fig. S4(c) and S5(c), ESI†).

Fig. S6 (ESI)† shows the removal kinetics of BrO_3^- (50 mg L^{-1}) by G-NZVI (200 mg L^{-1}) at four different pHs (4, 7, 9, and 11). The highest BrO_3^- removal was obtained at pH 7, whereas a sharp decline in the BrO_3^- removal rate occurred when pH values were higher and lower than 7. The zeta potential results (Fig. S7, ESI†) showed that a surface charge of G-NZVI became more negative from −3.41 mV to −30.7 mV as the suspension pH increased from 2 to 11. These results could be explained by an increase in the concentration of chloride or hydroxide (used for the pH adjustment) in the G-NZVI suspension because they can hinder the sorption of BrO_3^- on the reactive surface of G-NZVI and inhibit subsequent reductive removal of BrO_3^- on the surface.[41] The remarkable decline in the bromate removal at a pH higher than 7 could be caused by electrostatic repulsion between BrO_3^- and the more negatively charged G-NZVI surface.[42] Despite the relatively less negative charge on the G-NZVI surface at a lower pH (<7), the similar slow BrO_3^- removal kinetics on its surface might be attributed to the faster surface oxidation of iron nanoparticles under acidic environments.[43]

Conclusions

In this study, highly reactive and mobile G-NZVI nanoparticles with a diameter of 100–600 nm were synthesized for the complete reduction of BrO_3^- to Br^-. Excellent BrO_3^- removal (100%) was achieved in 2 min under aerobic conditions. The reduction kinetics of BrO_3^- by G-NZVI were much faster than any other reductants or catalysts reported previously. The outstanding characteristics of G-NZVI, such as high reactivity, mobility, and oxidation resistivity, are mainly attributed to the coating of the G-NZVI surface by polyphenols from the onion peel extract, resulting in the inhibition of the rapid surface oxidation of NZVI without lowering its reductive capacity, even under aerobic conditions. Previous studies have used plants as sources of polyphenol coating materials, however this study is the first investigation using onion peel waste for novel G-NZVI synthesis. Onion peel is one of the most widespread organic food waste materials worldwide; thus, the experimental results obtained in this study provide insight into the reuse of onion peel waste as a polyphenol coating material source for the synthesis of reactive nanomaterials, which can be applied to the reductive removal of contaminants from water and wastewater without needing to consider interference from oxygen during the treatment and remediation processes.

Conflicts of interest

There are no conflicts to declare.

Acknowledgements

This work has been supported by Nazarbayev University Research Grants (NLA: Contract No. 284-2019//012-2019 and CRP: 091019CRP2106). The authors would like to thank Prof. Seunghee Han of GIST for the basic training relating to environmental monitoring. The authors also would like to extend their gratitude to the anonymous reviewers that helped to significantly improve the quality of the paper.

References

1 F. Soltermann, C. Abegglen, C. Götz and U. Von Gunten, Bromide Sources and Loads in Swiss Surface Waters and Their Relevance for Bromate Formation during Wastewater Ozonation, *Environ. Sci. Technol.*, 2016, **50**, 9825–9834.
2 Y. Du, *et al.*, Genesis of salinized groundwater in quaternary aquifer system of coastal plain, Laizhou Bay, China: geochemical evidences, especially from bromine stable isotope, *Appl. Geochem.*, 2015, **59**, 155–165.
3 R. Li, C. Liu, P. Jiao and J. Wang, The tempo-spatial characteristics and forming mechanism of Lithium-rich brines in China, *Chin. Geol.*, 2018, **1**, 72–83.
4 U.S. Environmental Protection Agency, Proposed Guidelines for Carcinogen Risk Assessment, *Fed. Regist.*, 1996, **61**(79), 17960–18011.
5 R. Butler, A. Godley, L. Lytton and E. Cartmell, Bromate environmental contamination: review of impact and possible treatment, *Crit. Rev. Environ. Sci. Technol.*, 2005, **35**, 193–217.
6 M. Naushad, Z. A. Alothman, M. R. Khan and S. M. Wabaidur, Removal of Bromate from Water Using De-Acidite FF-IP Resin and Determination by Ultra-Performance Liquid Chromatography-Tandem Mass Spectrometry, *Clean: Soil, Air, Water*, 2013, **41**, 528–533.
7 Environmental Protection Agency (EPA), National Primary Drinking Water Regulations: Stage 2 Disinfectants and

Disinfection Byproducts Rule. U.S. Environmental Protection Agency, *Fed. Regist.*, 2006, **71**, 388–493.

8 A. Mills, A. Belghazi and D. Rodman, Bromate removal from drinking water by semiconductor photocatalysis, *Water Res.*, 1996, **30**, 1973–1978.

9 D. Barlokova, J. Ilavsky, I. Marko and J. Tkacova, Removal of bromates from water, *IOP Conf. Ser. Earth Environ. Sci.*, 2017, **92**, DOI: 10.1088/1755-1315/92/1/012021.

10 M. S. Elovitz, U. Von Gunten and H. P. Kaiser, Hydroxyl radical/ozone ratios during ozonation processes. II. The effect of temperature, pH, alkalinity, and DOM properties, *Ozone: Sci. Eng.*, 2000, **22**, 123–150.

11 A. A. Mohamed, M. Iwatsuki, T. Fukasawa and M. F. El-Shahat, Catalytic determination of vanadium using the perphenazine-bromate redox reaction and a citric acid activator, *Analyst*, 1995, **120**, 2281–2285.

12 M. O. Buffle, S. Galli and U. Von Gunten, Enhanced bromate control during ozonation: the chlorine-ammonia process, *Environ. Sci. Technol.*, 2004, **38**, 5187–5195.

13 R. Song, R. Minear, P. Westerhoff and G. Amy, Bromate formation and control during water ozonation, *Environ. Technol.*, 1996, **17**, 861–868.

14 U. von Gunten and J. Hoigné, Bromate Formation during Ozonization of Bromide-Containing Waters: Interaction of Ozone and Hydroxyl Radical Reactions, *Environ. Sci. Technol.*, 1994, **28**, 1234–1242.

15 B. Jung, R. Nicola, B. Batchelor and A. Abdel-Wahab, Effect of low- and medium-pressure Hg UV irradiation on bromate removal in advanced reduction process, *Chemosphere*, 2014, **117**, 663–672.

16 X. Liu, T. Zhang and Y. Shao, Aqueous bromate reduction by UV activation of sulfite, *Clean: Soil, Air, Water*, 2014, **42**, 1370–1375.

17 K. Y. Andrew Lin and S. Y. Chen, Bromate reduction in water by catalytic hydrogenation using metal-organic frameworks and sodium borohydride, *RSC Adv.*, 2015, **5**, 43885–43896.

18 K. Y. A. Lin and S. Y. Chen, Catalytic Reduction of Bromate Using ZIF-Derived Nanoscale Cobalt/Carbon Cages in the Presence of Sodium Borohydride, *ACS Sustainable Chem. Eng.*, 2015, **3**, 3096–3103.

19 L. Xie, C. Shang and Q. Zhou, Effect of Fe(III) on the bromate reduction by humic substances in aqueous solution, *J. Environ. Sci.*, 2008, **20**, 257–261.

20 L. Xie and C. Shang, Effects of copper and palladium on the reduction of bromate by Fe(0), *Chemosphere*, 2006, **64**, 919–930.

21 C. B. Wang and W. X. Zhang, Synthesizing nanoscale iron particles for rapid and complete dechlorination of TCE and PCBs, *Environ. Sci. Technol.*, 1997, **31**, 2154–2156.

22 H. Li, Y. S. Zhao, Z. T. Han and M. Hong, Transport of sucrose-modified nanoscale zero-valent iron in saturated porous media: role of media size, injection rate and input concentration, *Water Sci. Technol.*, 2015, **72**, 1463–1471.

23 W. Chen, X. Wang and Z. Yuan, Preparation of nanoscale zero-valent iron particles with different coatings for removal of Cr(VI) from water, *Int. J. Nanotechnol.*, 2016, **13**, 923–934.

24 M. A. Kumar, S. Bae, S. Han, Y. Chang and W. Lee, Reductive dechlorination of trichloroethylene by polyvinylpyrrolidone stabilized Fe-Ni nano-particles, *J. Hazard. Mater.*, 2017, **340**, 399–406.

25 Y. P. Sun, X. Q. Li, W. X. Zhang and H. P. Wang, A method for the preparation of stable dispersion of zero-valent iron nanoparticles, *Colloids Surf., A*, 2007, **308**, 60–66.

26 E. C. Njagi, *et al.*, Biosynthesis of iron and silver nanoparticles at room temperature using aqueous sorghum bran extracts, *Langmuir*, 2011, **27**, 264–271.

27 C. Mystrioti, *et al.*, Assessment of polyphenol coated Nano zero Valent iron for hexavalent chromium removal from contaminated waters, *Bull. Environ. Contam. Toxicol.*, 2015, **94**, 302–307.

28 S. Iravani, Green synthesis of metal nanoparticles using plants, *Green Chem.*, 2011, **13**, 2638–2650.

29 S. S. Chen, H. D. Hsu and C. W. Li, A new method to produce nanoscale iron for nitrate removal, *J. Nanopart. Res.*, 2004, **6**, 639–647.

30 K. Sohn, S. W. Kang, S. Ahn, M. Woo and S. K. Yang, Fe(0) nanoparticles for nitrate reduction: stability, reactivity, and transformation, *Environ. Sci. Technol.*, 2006, **40**, 5514–5519.

31 S. Eslami, M. A. Ebrahimzadeh and P. Biparva, Green synthesis of safe zero valent iron nanoparticles by: Myrtus communis leaf extract as an effective agent for reducing excessive iron in iron-overloaded mice, a thalassemia model, *RSC Adv.*, 2018, **8**, 26144–26155.

32 N. Horzum, M. M. Demir, M. Nairat and T. Shahwan, Chitosan fiber-supported zero-valent iron nanoparticles as a novel sorbent for sequestration of inorganic arsenic, *RSC Adv.*, 2013, **3**, 7828–7837.

33 F. Paquin, J. Rivnay, A. Salleo, N. Stingelin and C. Silva, Multi-phase semicrystalline microstructures drive exciton dissociation in neat plastic semiconductors, *J. Mater. Chem. C*, 2015, **3**, 10715–10722.

34 Y. Sihn, S. Bae and W. Lee, Immobilization of uranium(VI) in a cementitious matrix with nanoscale zerovalent iron (NZVI), *Chemosphere*, 2019, **215**, 626–633.

35 B. Desalegn, M. Megharaj, Z. Chen and R. Naidu, Green synthesis of zero valent iron nanoparticle using mango peel extract and surface characterization using XPS and GC-MS, *Heliyon*, 2019, **5**, e01750.

36 D. Briggs, D. Clarke, S. Suresh, I. Ward and M. Black, *Surface Analysis of Polymers by XPS and Static SIMS*, Cambridge University Press, 2009.

37 V. T. Padil Vinod, *et al.*, Gum karaya (Sterculia urens) stabilized zero-valent iron nanoparticles: characterization and applications for the removal of chromium and volatile organic pollutants from water, *RSC Adv.*, 2017, **7**, 13997–14009.

38 K. A. Lee, *et al.*, Antioxidant activities of onion (Allium cepa L.) peel extracts produced by ethanol, hot water, and subcritical water extraction, *Food Sci. Biotechnol.*, 2014, **23**, 615–621.

39 N. C. Mueller, *et al.*, Application of nanoscale zero valent iron (NZVI) for groundwater remediation in Europe, *Environ. Sci. Pollut. Res.*, 2012, **19**, 550–558.

40 H. Chen, *et al.*, Aqueous bromate reduction by catalytic hydrogenation over Pd/Al2O3 catalysts, *Appl. Catal., B*, 2010, **96**, 307–313.

41 P. A. Sundaram, R. Augustine and M. Kannan, Extracellular biosynthesis of iron oxide nanoparticles by Bacillus subtilis strains isolated from rhizosphere soil, *Biotechnol. Bioprocess Eng.*, 2012, **17**, 835–840.

42 S. S. Poguberović, *et al.*, Removal of As(III) and Cr(VI) from aqueous solutions using 'green' zero-valent iron nanoparticles produced by oak, mulberry and cherry leaf extracts, *Ecol. Eng.*, 2016, **90**, 42–49.

43 C. Wu, *et al.*, The double influence mechanism of pH on arsenic removal by nano zero valent iron: electrostatic interactions and the corrosion of Fe0, *Environ. Sci.: Nano*, 2017, **4**, 1544–1552.

44 X. Xin, *et al.*, Simultaneous adsorption/reduction of bromate in water using nano zero-valent iron supported on ordered mesoporous silica, *Water Sci. Technol.: Water Supply*, 2019, **19**, 1330–1338.

45 Q. Wang, S. Snyder, J. Kim and H. Choi, Aqueous ethanol modified nanoscale zerovalent iron in bromate reduction: synthesis, characterization, and reactivity, *Environ. Sci. Technol.*, 2009, **43**, 3292–3299.